Biomaterials 30 (2009) 6768–6779

Contents lists available at ScienceDirect

Biomaterials

journal homepage: www.elsevier.com/locate/biomaterials

The effects of rhBMP-2 released from biodegradable polyurethane/microsphere composite scaffolds on new bone formation in rat femora

Bing Li [a,b,1], Toshitaka Yoshii [b,c,2], Andrea E. Hafeman [a,b,3], Jeffry S. Nyman [b,c,d,4], Joseph C. Wenke [e,5], Scott A. Guelcher [a,b,*]

[a] Department of Chemical and Biomolecular Engineering, Vanderbilt University, 2301 Vanderbilt Place, VU Station B #351604, Nashville, TN 37235, USA
[b] Center for Bone Biology, Vanderbilt University Medical Center, Nashville, TN, USA
[c] Department of Orthopaedics and Rehabilitation, Vanderbilt University Medical Center, 1215 21st Avenue South, Room 4200, Nashville, TN 37232-8774, USA
[d] Department of Veterans Affairs, Tennessee Valley Healthcare System, 1215 21st Avenue South, Room 4200, Nashville, TN 37232-8774, USA
[e] Regenerative Medicine Task Area, US Army Institute of Surgical Research, 3400 Rawley E. Chambers Avenue, Fort Sam Houston, TX, USA

ARTICLE INFO

Article history:
Received 18 June 2009
Accepted 26 August 2009
Available online 17 September 2009

Keywords:
BMP (bone morphogenetic protein)
Bone regeneration
Drug delivery
In vivo test
Polyurethane

ABSTRACT

Scaffolds prepared from biodegradable polyurethanes (PUR) have been investigated as a supportive matrix and delivery system for skin, cardiovascular, and bone tissue engineering. While previous studies have suggested that PUR scaffolds are biocompatible and moderately osteoconductive, the effects of encapsulated osteoinductive molecules, such as recombinant human bone morphogenetic protein (rhBMP-2), on new bone formation have not been investigated for this class of biomaterials. The objective of this study was to investigate the effects of different rhBMP-2 release strategies on new bone formation in PUR scaffolds implanted in rat femoral plug defects. In the simplest approach, rhBMP-2 was added as a dry powder prior to the foaming reaction, which resulted in a burst release of 35% followed by a sustained release for 21 days. Encapsulation of rhBMP-2 in either 1.3-micron or 114-micron PLGA microspheres prior to the foaming reaction reduced the burst release. At 4 weeks post-implantation, all rhBMP-2 treatment groups enhanced new bone formation relative to the scaffolds without rhBMP-2. Scaffolds incorporating rhBMP-2 powder promoted the most extensive new bone formation, while scaffolds incorporating rhBMP-2 encapsulated in 1.3-micron microspheres, which exhibited the lowest burst release, promoted the least extensive new bone formation. Thus our observations suggest that an initial burst release followed by sustained release is better for promoting new bone formation.

1. Introduction

Incorporation of signaling molecules, such as growth factors, in a scaffold to support ingrowth of cells and new tissue is an effective approach to regenerating tissue such as bone. Polymer scaffolds have been used extensively in bone tissue engineering. Ideally, the scaffold should support cell attachment and ingrowth of new tissue, as well as biodegrade at a rate matching that of new tissue ingrowth.

Scaffolds synthesized from biodegradable polyurethanes (PUR) have been investigated in skin [1–3], cardiovascular [4–7], and bone [8,9] tissue engineering applications. In these applications, PUR scaffolds have been reported to support cell ingrowth and tissue remodeling, as well as biodegrade to non-cytotoxic decomposition products [3,4,10–12]. A distinguishing feature of these biomaterials is the potential to inject them as a reactive two-component liquid or paste that cures *in situ* to form a solid elastomeric scaffold without causing tissue damage or inducing a significant inflammatory response [1,9,13,14]. PUR scaffolds have also been investigated as delivery systems for controlled release of growth factors, including bFGF and rhPDGF-BB [2,13,15]. We have previously demonstrated that rhPDGF-BB released from two-component reactive PUR scaffolds implanted in rat skin excisional wounds both enhanced new tissue formation and also accelerated polymer degradation, suggesting that the bioactivity of the growth factor was not adversely affected by the chemical reaction [2].

* Corresponding author. Department of Chemical and Biomolecular Engineering, Vanderbilt University, 2301 Vanderbilt Place, VU Station B #351604, Nashville, TN 37235. Tel.: +1 615 322 9097; fax: +1 615 343 7951.
E-mail addresses: bing.li@vanderbilt.edu (B. Li), toshitaka.yoshii@vanderbilt.edu (T. Yoshii), andrea.e.hafeman@vanderbilt.edu (A.E. Hafeman), jeffry.s.nyman@Vanderbilt.Edu (J.S. Nyman), joseph.wenke@us.army.mil (J.C. Wenke), scott.guelcher@vanderbilt.edu (S.A. Guelcher).
[1] Tel.: +1 615 322 9097; fax: +1 615 343 7951.
[2] Tel.: +1 615 936 0363; fax: +1 615 343 3815.
[3] Tel.: +1 615 322 9097; fax: +1 615 343 7951.
[4] Tel.: +1 615 936 6296; fax: +1 615 343 1098.
[5] Tel.: +1 210 913 3742; fax: +1 210 916 3877.

0142-9612/$ – see front matter © 2009 Elsevier Ltd. All rights reserved.
doi:10.1016/j.biomaterials.2009.08.038

Report Documentation Page

Form Approved
OMB No. 0704-0188

1. REPORT DATE	2. REPORT TYPE	3. DATES COVERED
01 DEC 2009	**N/A**	**-**

4. TITLE AND SUBTITLE	5a. CONTRACT NUMBER
The effects of controlled release of BMP-2 from biodegradable polyurethane/microsphere composite scaffolds on new bone formation in a rat femoral plug model.	5b. GRANT NUMBER
	5c. PROGRAM ELEMENT NUMBER
6. AUTHOR(S)	5d. PROJECT NUMBER
Li B., Yoshii T., Hafeman A. E., Nyman J. S., Wenke J. C., Guelcher S. A.,	5e. TASK NUMBER
	5f. WORK UNIT NUMBER
7. PERFORMING ORGANIZATION NAME(S) AND ADDRESS(ES)	8. PERFORMING ORGANIZATION REPORT NUMBER
United States Army Institute of Surgical Research, JBSA Fort Sam Houston, TX 78234	
9. SPONSORING/MONITORING AGENCY NAME(S) AND ADDRESS(ES)	10. SPONSOR/MONITOR'S ACRONYM(S)
	11. SPONSOR/MONITOR'S REPORT NUMBER(S)

12. DISTRIBUTION/AVAILABILITY STATEMENT
Approved for public release, distribution unlimited

13. SUPPLEMENTARY NOTES

14. ABSTRACT

15. SUBJECT TERMS

16. SECURITY CLASSIFICATION OF:			17. LIMITATION OF ABSTRACT	18. NUMBER OF PAGES	19a. NAME OF RESPONSIBLE PERSON
a. REPORT	b. ABSTRACT	c. THIS PAGE			
unclassified	**unclassified**	**unclassified**	**UU**	**12**	

The osteoinductive growth factor bone morphogenetic protein-2 (BMP-2) stimulates osteoblast differentiation and promotes bone formation. Recombinant human (rh) BMP-2 delivered from a collagen sponge (INFUSE® Bone Graft, Medtronic) is an FDA-approved therapy for posterior-lateral spine, tibia, and specific craniofacial applications. The collagen sponge delivery system results in a bolus release of growth factor in the first several hours [16]. Unfortunately, there is no conclusive evidence regarding the optimal release kinetics. There is, however, evidence that BMP-2 promotes bone formation via different mechanisms such as osteoblast differentiation, chemoattraction, angiogenesis, and cell signaling at the initiation of fracture healing. A number of studies have suggested that sustained release of rhBMP-2 [17–19] is more effective than a bolus release for promoting new bone formation. For example, delayed percutaneous injection of rhBMP-2 into the fracture site one week after surgery resulted in enhanced fracture healing relative to injection within one day in a primate model [20]. The improvement in healing associated with delayed injection was conjectured to result from a larger number of cells at the fracture site. Other studies have suggested that BMP-2 plays an important role at early stages in the healing process. BMP-2 is involved in promoting angiogenesis [21] and migration of human mesenchymal progenitor cells (MPCs) [22]. It may also serve as the trigger in the fracture healing cascade as demonstrated by its early maximal expression on day 1 as measured in a mouse tibia fracture model [23]. Taken together, these previous studies suggest that both a burst and sustained release of rhBMP-2 are beneficial. A burst release of rhBMP-2 is anticipated to increase cellular migration and promote angiogenesis, while sustained release is anticipated to promote differentiation of the responding cells and thus more new bone formation.

One purpose of the present study was to evaluate the ability of rhBMP-2 delivered from PUR scaffolds to heal bone defects. Scaffolds fabricated from biodegradable segmented PUR elastomers supported new bone formation when implanted in monocortical defects in the iliac crest of sheep for six months [8,24], implying that the materials are moderately osteoconductive. Delivery of rhBMP-2 from polymeric scaffolds, such as poly(lactic-co-glycolic acid) (PLGA) and poly(propylene fumarate) (PPF), has been shown to promote new bone formation [25–31], but the effects of rhBMP-2 released from two-component reactive polyurethanes on new bone formation have not been investigated. It has been suggested that the harsh polymerization conditions, such as crosslinking and thermal gradients, associated with reactive biomaterials may adversely affect the bioactivity of added growth factors [32]. Although we have previously shown that rhPDGF powder encapsulated in reactive PUR scaffolds retained ~80% of its bioactivity [2], these results do not necessarily translate to rhBMP-2. Another objective of this study was to modulate the release kinetics by encapsulating rhBMP-2 in microspheres of varying size prior to embedding in the PUR scaffolds. The burst release from microspheres in the range of 35–45 μm reportedly decreased when embedded in PPF/microsphere composite scaffolds [32]. However, the effects of particle size on release kinetics and new bone formation have not been previously investigated. In this study, we have investigated the effects of microsphere size on rhBMP-2 release kinetics and new bone formation in a rat femoral plug model.

2. Materials and methods

2.1. Materials

Polyvinyl alcohol (PVA), glycolide, and D,L-lactide were obtained from Polysciences (Warrington, PA). The tertiary amine catalyst TEGOAMIN33, which comprised a solution of 33 wt% triethylene diamine (TEDA) in dirpropylene glycol, was received from Goldschmidt (Hopewell, VA) as a gift. Polyethylene glycol (PEG, 600 Da) was purchased from Alfa Aesar (Ward Hill, MA). Dichloromethane (DCM) and glucose were from Acros Organics (Morris Plains, NJ). Hexamethylene diisocyanate trimer (HDIt, Desmodur N3300A) was received as a gift from Bayer Material Science (Pittsburgh, PA). Stannous octoate catalyst was received from Nusil technology (Overland Park, KS). α-minimal essential medium (α-MEM) was purchased from Fisher Scientific (Pittsburgh, PA). PLGA (50/50, intrinsic viscosity 0.58 dL/g) was purchased from LACTEL (Pelham, AL). Recombinant human bone morphogenetic protein-2 (rhBMP-2) was received as a gift from Professor Jeffrey Hollinger at Carnegie Mellon University. All other reagents were purchased from Sigma–Aldrich (St. Louis, MO).

2.2. Poly(lactic-co-glycolic acid) (PLGA) microspheres fabrication

A double emulsion technique was used to fabricate PLGA microspheres [2,33]. PLGA (50/50, 0.58 dL/g) and PEG (4600 Da), at a ratio of 9:1, were dissolved in DCM at polymer concentrations of 10% and 5% for large and small size particles, respectively. A glucose solution of BSA–FITC (fluoroisothiocyanate-labeled bovine serum albumin) or rhBMP-2 was added to the polymer DCM solution, followed by sonication to form the water-in-oil (w/o) emulsion. The w/o emulsion was then added to a PVA solution (0.3% and 5% for large and small size particles, respectively) under intense stirring to form the water-in-oil-in-water (w/o/w) double emulsion. A homogenizer was used for the first 100 s of stirring. Subsequently, the double emulsion was mixed using a stir bar for another 2.5 h to evaporate the DCM solvent.

The particles were then recovered by centrifugation, washed, and lyophilized. Large microspheres (PLGA-L) were imaged using an Olympus BX60 microscope, and the particle size distribution (PSD) was calculated by sampling ~500 particles. Small microspheres (PLGA-S) were imaged by scanning electron microscopy (Hitachi S-4200 SEM), and the PSD determined by dynamic laser light scattering (Malvern ZetaSizer 3000HS). The loading efficiency of rhBMP-2 into PLGA particles was determined as reported previously in Ref. [18]. Briefly, the microspheres were dissolved in DCM, rhBMP-2 was extracted into PBS over a period of 36 h, and the concentration of rhBMP-2 was then measured by ELISA. The thermal transition of as-received PLGA and PLGA particles were measured using a Thermal Analysis Q2000 Differential Scanning Calorimeter (DSC). Two cycles of cooling and heating in the temperature range of −50 °C and 150 °C, at a speed of 10 °C/min, were recorded for 5 mg samples.

2.3. Synthesis and characterization of polyurethane (PUR) scaffolds

Polyester triols (900 Da) were prepared from a glycerol starter and a backbone comprising 60 wt% ε-caprolactone, 30 wt% glycolide, and 10 wt% D,L-lactide as published previously in Refs. [10,12]. PUR scaffolds were synthesized by one-shot reactive liquid molding of hexamethylene diisocyanate trimer (HDIt; Desmodur N3300A) and a hardener comprising 900-Da polyol (or a 50/50 w/w mixture of polyester triol and PEG600), 1.5 parts per hundred parts polyol (pphp) water, 4.5 pphp TEGOAMIN33 tertiary amine catalyst, 1.5 pphp sulfated castor oil stabilizer, and 4.0 pphp calcium stearate pore opener. The isocyanate was added to the hardener, mixed for 30 s in a Hauschild SpeedMixer™ DAC 150 FVZ-K vortex mixer (FlackTek, Inc., Landrum, SC), and the resulting liquid mixture poured into a cylindrical mold where it cured as a free-rise foam after ~20 min [10,12]. The targeted index (the ratio of NCO to OH equivalents × 100) was 100 for PUR scaffolds incorporating small PLGA particles and 115 for all other scaffolds. In order to incorporate protein into PUR scaffold, lyophilized protein powder, PLGA-L, or PLGA-S was added to the hardener component before mixing with the isocyanate to prepare the scaffolds. Specific formulations evaluated are listed in Table 1. For each of the three delivery strategies, the dosage of rhBMP-2 was controlled at 2.5 μg/ml scaffold.

Scanning electron microscopy (Hitachi S-4200 SEM, Finchampstead, UK) was utilized to measure the pore size and determine the internal pore morphology of the polyurethane scaffolds. The density and core porosity were calculated as reported previously in Ref. [2,10], with three replicates for each PUR type. The thermal transitions of scaffolds were measured using a Thermal Analysis Q2000 Differential Scanning Calorimeter (DSC). Two cycles of cooling and heating in the temperature range of −50 °C and 150 °C, at a speed of 10 °C/min, were recorded for 5 mg samples. The storage and loss moduli of the scaffolds were also evaluated by dynamic

Table 1
Summary of PUR compositions. The formulation of the proteins added to the hardener component is listed for each material.

PUR type	Additives in the hardener
PUR	N/A
PUR/rhBMP-2	rhBMP-2/heparin (1:20) powder, 2 wt% Glucose
PUR/PLGA-L-rhBMP-2	PLGA-L-rhBMP-2, 14 wt%
PUR/PLGA-S-rhBMP-2	PLGA-S-rhBMP-2, 9 wt%
PUR/BSA–FITC	BSA–FITC powder, 2 wt% Glucose
PUR/PLGA-L-BSA–FITC	PLGA-L-BSA–FITC, 14 wt%
PUR/PLGA-S-BSA–FITC	PLGA-S-BSA–FITC, 9 wt%

mechanical analysis (DMA) in compression mode with a temperature sweep of −80–100 °C, at a frequency of 1 Hz, 20-μm amplitude, 0.3-% strain, and 0.2-N static force [2,13]. Confocal microscopy was performed using a Zeiss LSM510 confocal microscope to the image distribution of BSA–FITC within the microspheres and scaffolds.

The temperature profiles during foaming of the polyurethane scaffolds were measured to determine the exotherm from the reaction. After the isocyanate and resin components (with or without microspheres) were combined, a thermocouple (Fluke 53II) was inserted into the center of the reactive liquid mixture for the duration of foaming. The temperature was recorded every 15 or 30 s.

2.4. In vitro release experiment

Three replicate scaffold samples (~50 mg) containing 2.5 μg rhBMP-2 were immersed in 1 ml release medium (α-MEM incorporating 1% BSA) contained in polypropylene vials sealed by O-rings. BSA was included to minimize adsorption of rhBMP-2 onto the scaffolds and vials [2]. The medium was refreshed every 24 h to minimize degradation of the growth factor [2]. The rhBMP-2 concentration of daily pools as indicated in the cumulative release plot was determined using a Human BMP-2 Quantikine ELISA kit (R&D systems, Minneapolis, MN). The daily release plot was generated from a logarithm curve fit from the raw data. The power law model [34,35] was used to fit the accumulative release curves in order to elucidate the drug release mechanism.

2.5. In vitro alkaline phosphatase (ALP) activity assay

The releasates from the first 9 days from PUR/rhBMP-2 and PUR/PLGA-L-rhBMP-2 separately were combined and examined for ALP activity using MC3T3 osteoprogenitor cells. MC3T3 cells were plated on 48-well plates in α-MEM containing 10% FBS. When the cells reached confluence, the culture medium was changed to α-MEM containing 2.5% FBS with or without 100 ng/ml of rhBMP-2 releasate. Fresh rhBMP-2 was used as a positive control. The cell culture medium was changed every two days. At days 3 and 7, cells were washed with phosphate-buffered saline and lysed with 80 μl of 0.05% Triton X-100. The plates were then subjected to three freeze/thaw cycles. The lysates (20 μl) were added to 100 μl of substrate buffer (2 mg/ml disodium p-nitrophenylphosphate hexahydrate and 0.75 M 2-amino-2-methyl-1-propanol). After incubation of the mixtures at 37 °C for 30 min, absorbance at 405 nm was measured. ALP activity was determined from a standard curve generated by employing the reaction of a p-nitrophenyl solution. The ALP activity was normalized by the total protein content determined using the BCA assay (Pierce). One way ANOVA with bonferroni correction ($p < 0.05$) was used for evaluation of statistical significance.

2.6. In vivo evaluation of rhBMP-2 implants in a rat femoral plug defect model

All surgical procedures were reviewed and approved by the Institutional Animal Care and Use Committee. Male Sprague–Dawley rats (Harlan Labs) aged 8 weeks (200–250 g) were used for this study. A monocortical plug bone defect (3 mm diameter × 5 mm deep) was created in the distal region of the femur diaphysis [36], and a cylindrical PUR scaffold (3 × 5 mm) was implanted into the defect. Treatment groups included PUR (without rhBMP-2 as a control), PUR/rhBMP-2, PUR/PLGA-L-rhBMP-2, and PUR/PLGA-S-rhBMP-2 ($n = 6$). The dosage of rhBMP-2 within each experimental scaffold was 2 μg (60 μg rhBMP-2/ml scaffold). After two and four weeks post-implantation, the rats were sacrificed and the femurs removed and fixed in 10% phosphate-buffered formalin.

Quantitative 3D analysis of bone ingrowth in the scaffolds was performed using a μCT40 (SCANCO Medical, Bassersdorf, Switzerland), at a voxel size of 24 mm (isotropic). The X-ray source settings were 55 kVp and 145 mA with an integration time of 300 ms. The region of interest (100 axial slices) was centered over the defect site in the distal femur. After reconstruction, the bone tissue was segmented from air or soft tissue using a threshold of 270 per thousand (or 438.7 mgHA/cm^3), a Gaussian noise filter of 0.8, and support of 2. This threshold was consistent through all specimens. Utilizing the Scanco evaluation software, we quantified the amount of bone ingrowth into the scaffold as the percentage of bone volume (BV) per total volume (TV), in which TV was generated by measuring the contour of the defect site. Because the μCT40 is calibrated to known densities of hydroxyapatite (phantom),

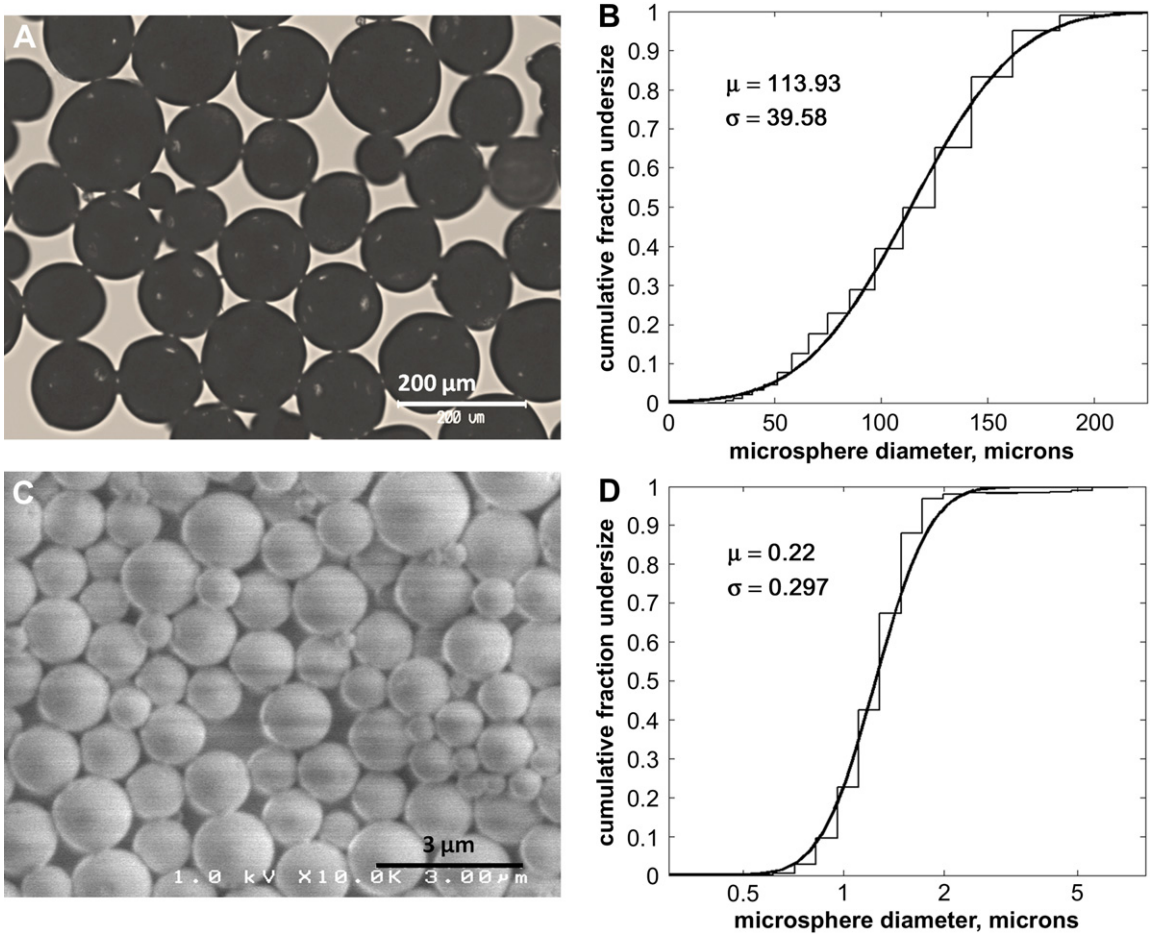

Fig. 1. PLGA particles characterization: imaging and size distribution. (A) imaging of PLGA-L by light microscope, (B) particle size distribution of PLGA-L (light microscopy), (C) imaging of PLGA-S by SEM, and (D) particle size distribution of PLGA-S (Malvern Zetasizer).

Table 2
Summary of properties of PLGA microspheres.

	Average size (μm)	Std DEV (μm)	PEG content (NMR)	Yield	Initial rhBMP-2 loading (μg/ml)	Encapsulation efficiency	T_g (DSC)
PLGA-L	114	40	6.7%	79.5%	1.79	78.3%	34.4 °C
PLGA-S	1.30	0.39	0.11%	80.3%	2.77	65.2%	45.9 °C

the mineral density (mgHA/cm^3) of each voxel was automatically provided for segmented bone. We recorded the mean volumetric bone density of the mineralized tissue (mBMD) in the metaphysis.

Rat bones were then decalcified with 10% ethylenediaminetetraacetic acid (EDTA; Invitrogen), dehydrated, embedded in paraffin, and sectioned at 5 μm thickness. The coronal slice sections were stained with hematoxylin and eosin (H&E). Specimens were examined under light microscopy. The amount of bone ingrowth in the scaffolds was quantified at the center sections of the implants [37]. The area of bone ingrowth in the scaffolds was highlighted using adobe photoshop elements 7.0 and measured using image analysis software (Scion Image, Scion Corp., Frederick, MD), and the ratio of bone ingrowth area per whole implant area was evaluated. One way ANOVA with bonferroni correction ($p < 0.05$) was used for evaluation of statistical significance for both μCT imaging and histomorphometry analysis.

3. Results

3.1. Characterization of PLGA microphores

PLGA microspheres were fabricated using a double emulsion technique. Previous studies have shown that the activity of released rhBMP-2 is not adversely affected by the presence of the DCM solvent used in the double emulsion technique [38], and the NMR spectra indicated that no residual DCM solvent was present in the microspheres (data not shown). Images of PLGA-L (light microscopy) and PLGA-S (SEM) microspheres are shown in Fig. 1A and C. PLGA-L microspheres fit a normal distribution (Fig. 1B), with an average size of 114 ± 40 μm (Table 2). Interestingly, the PLGA-S microspheres fit a log-normal distribution (Fig. 1D), with an average size of 1.30 ± 0.39 μm (Table 2). While both formulations incorporated 10% PEG4600 prior to formation of the microspheres, the PLGA-S and PLGA-L microspheres contained varying amounts of PEG due to differences in PEG encapsulation efficiency. As measured by ^{1}H NMR, PLGA-L microspheres had higher PEG content (6.7 wt%) compared to the PLGA-S (0.11 wt%) (Table 2). The DSC data (Fig. 2) show that the PLGA microspheres undergo a single glass transition temperature, suggesting that the microspheres are phase-mixed. This observation is consistent with a previous study showing that blends of PLGA and PEG (10,000 g/mol) are miscible when solvent-cast from a solution in chloroform [39]. Due to the differences in PEG content, the PLGA-L microspheres had a lower T_g (34.4 °C, Table 2) compared to the PLGA-S microspheres (45.9 °C). This observation is consistent with the well-known Fox equation, which predicts the glass transition temperature of polymer blends $T_{g,B}$ as a function of the weight fraction w_i of each component:

$$1/T_{g,B} = w_1/T_{g1} + w_2/T_{g2} \quad (1)$$

Considering that the T_g of the pure PLGA and the pure PEG components were 41.5 °C and −22 °C [40], respectively, the Fox equation predicts T_g values of 41.4 °C and 34.0 °C for the PLGA-S and PLGA-L microspheres. The value of $T_g = 34.0$ °C predicted from the Fox equation is in good agreement with the experimental value of 34.4 °C (Table 2) for the PLGA-L microspheres. However, for the PLGA-S microspheres, the measured value of T_g (45.9 °C) exceeds that of the pure PLGA used to fabricate the microspheres. It is conjectured that the increase in T_g of the PLGA-S microspheres results from the incorporation of poly(vinyl alchol) (PVA) stabilizer, which has $T_g = 85$ °C (as indicated in the product specification). In order to prepare a stable suspension of ∼1 μm microspheres, a higher concentration of PVA stabilizer in the aqueous phase was required for the PLGA-S microspheres. Although the concentration of PVA in the PLGA microspheres could not be determined from the NMR spectra due to overlapping peaks with PEG and PLGA, it is likely that the PVA content was higher in the PLGA-S microspheres due to the higher concentration of PVA in the aqueous phase and larger surface-to-volume ratio.

For both PLGA-L and PLGA-S formulations, the overall yield of microspheres was ∼80% as shown in Table 2. However, the rhBMP-2

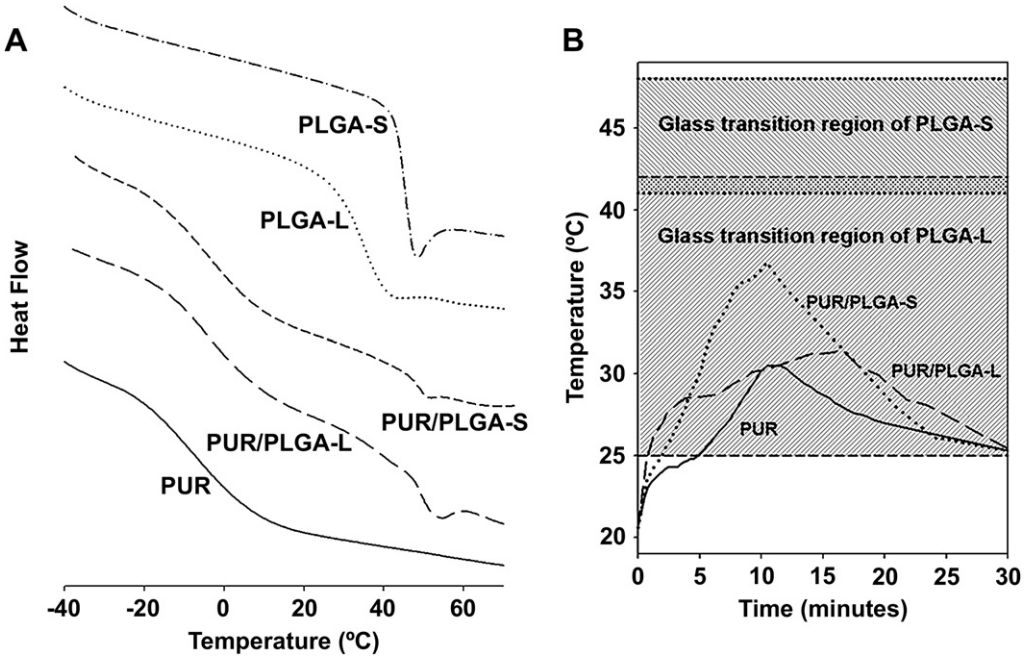

Fig. 2. (A) DSC profiles of PUR scaffolds and PLGA microspheres and (B) temperature profile during the polymerization reaction. The glass transition regions for PLGA-L and PLGA-S microspheres are indicated by the hatched lines on the plot.

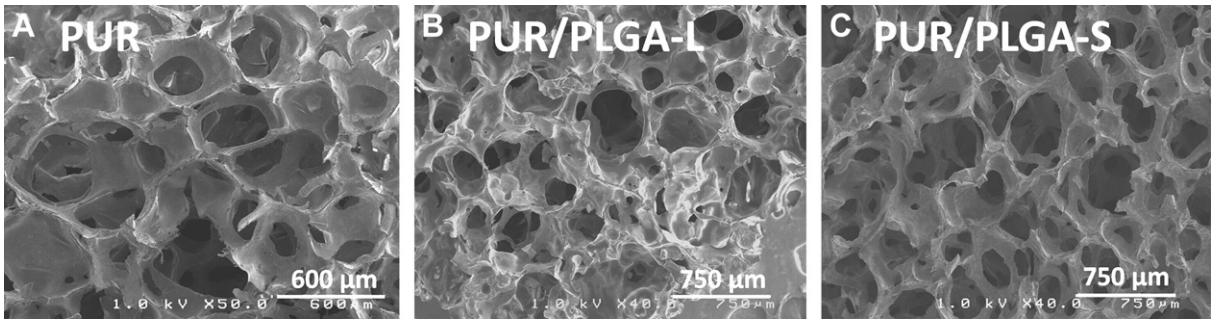

Fig. 3. SEM images of PUR scaffolds incorporating FITC–BSA: (A) BSA–FITC added as a lyophilized powder, (B) BSA–FITC microencapsulated in PLGA-L microspheres, and (C) BSA–FITC microencapsulated in PLGA-S microspheres.

encapsulation efficiency for PLGA-L microspheres was significantly higher than that measured for the PLGA-S microspheres (78.3 and 65.2%, respectively). Furthermore, when the concentration of PLGA-S microspheres in the PUR scaffolds exceeded 10 wt%, the materials became unstable, exhibiting large voids. Therefore, to maintain the targeted 2.5 μg rhBMP-2/scaffold loading, the loading of rhBMP-2 in the PLGA-S microspheres was higher than that of PLGA-L microspheres (Table 2).

3.2. Synthesis and characterization of PUR scaffolds

Two-component porous PUR scaffolds synthesized by reactive liquid molding exhibited interconnected pores as evidenced by SEM imaging (Fig. 3A). The pore size was in the range of 200–600 μm and the thickness of the pore walls and struts was less than ~100 μm thick. The incorporation of PLGA-S microspheres did not substantially change the pore morphology (Fig. 3B and C), but the presence of PLGA-L microspheres in the scaffold resulted in more irregular pore shapes. The porosity of the blank PUR scaffolds was calculated from the density to be 92.9%, and although there was a significant reduction in porosity associated with the addition of PLGA microspheres, the decrease in porosity was small, ranging from 2.0 to 2.5% (Table 3).

DSC scans for PUR, PLGA-S, PLGA-L, PUR/PLGA-S, and PUR/PLGA-L are shown in Fig. 2. The glass transition temperatures (calculated as the midpoint of the glass transition region from the DSC scan) are listed in Table 3. PUR scaffolds without microspheres exhibited a single T_g of −8.6 °C, which suggests phase mixing of the isocyanate and polyol components consistent with our previous studies [10,13]. As shown in Fig. 2 and Table 3, the addition of PLGA microspheres resulted in a phase-separated polymer blend with two T_gs, one corresponding to the PUR component at about −5 °C and one corresponding to the PLGA component at 40–45 °C. Interestingly, when the PUR/PLGA scaffolds were heated to 55 °C (just above T_g), quenched to −50 °C, and re-heated to 55 °C, the materials exhibited only one T_g that was intermediate between that of the PUR scaffold and PLGA microspheres (Table 3). This observation suggests that the PLGA and PUR polymers are miscible, which is not surprising considering that the PUR contains a polyester soft segment. The reaction exotherm is plotted in Fig. 2B. When the reaction is initiated at ambient (e.g., 20–23 °C) conditions, the maximum temperature attained for PUR/PLGA-L scaffolds is ~32 °C and the material cools to ambient temperature after 30 min. Superimposed on the reaction exotherms are the glass transition regions measured for PLGA-S and PLGA-L microspheres. Interestingly, the glass transition region for the PLGA-L microspheres overlaps with the reaction exotherm, suggesting that the PLGA-L microspheres may soften during the reaction, thereby promoting inter-penetration of PUR and PLGA chains at the interface. The modest shift in T_g from −8.6 °C for the blank PUR scaffold to −4.8 °C for the PUR/PLGA-L scaffold further suggests that the reaction exotherm promoted softening and mixing near the surface of the PLGA-L microspheres.

DMA temperature sweeps were typical of rubbery elastomers as reported previously in Refs.[2,13], exhibiting a glassy region below T_g, a glass transition region, and a rubbery plateau at temperatures above T_g. The storage moduli at 37 °C were measured to be 0.82 MPa, 2.31 MPa, and 0.54 MPa for PUR, PUR/PLGA-L, and PUR/PLGA-S, respectively (Table 3). The incorporation of PLGA-L microspheres increased the storage modulus significantly, while the presence of PLGA-S microspheres decreased the storage modulus. The effects of PLGA-S microspheres on mechanical properties are consistent with a previous study showing that the compressive modulus of poly(propylene fumarate) (PPF) scaffolds decreased when 35–45 μm microspheres were embedded in the scaffold [32].

Table 3
Physical and mechanical properties of PUR scaffolds. E' represents the storage modulus measured by DMA.

PUR type ($n=3$)	Density (kg m^{-3})	Porosity (vol-%)	T_g (°C) DSC 1st cycle)	T_g (°C) DSC 2nd cycle	E' at 37 °C (MPa)
PUR	86.6 ± 2.7	92.9 ± 0.2	−8.6	−8.6	0.82 ± 0.35
PUR/PLGA-L	116.7 ± 2.7	90.4 ± 0.2	−4.8, 39.5	1.9	2.31 ± 0.28
PUR/PLGA-S	110.2 ± 2.5	90.9 ± 0.2	−5.2, 44.5	−4.8	0.54 ± 0.13

3.3. Distribution of protein in microspheres and polyurethane scaffolds

Confocal microscopy [32] was used to image the distribution of the model BSA–FITC protein in the microspheres and scaffolds. For both PLGA-L-BSA–FITC and PLGA-S-BSA–FITC microspheres, the protein appeared to be more concentrated near the surface of the microspheres (Fig. 4B, C). For PUR/BSA–FITC scaffolds, the BSA–FITC powder was distributed uniformly throughout the pore walls of the scaffold (compare Fig. 4D to the blank PUR scaffolds in Fig. 4A). However, the confocal images suggest that the particle size distribution was rather broad, which is conjectured to result from poor dispersion of the hydrophilic lyophilized rhBMP-2/glucose powder in the hydrophobic polymer. For PUR/PLGA-L-BSA–FITC scaffolds (Fig. 4E), since the wall of the scaffold was in most cases less than ~100 μm thick (Fig. 4D), many of the particles were only partially embedded in the scaffold. In some cases the PLGA-L microspheres appeared to thicken the pore walls and struts, which is conjectured to reinforce the mechanical properties of the PUR/PLGA-L scaffolds. In contrast, due to their smaller size, PLGA-S-BSA–FITC particles were completely embedded and uniformly distributed throughout the pore walls of the scaffold (Fig. 4F). Furthermore, the small particles appeared to be well-dispersed and did not aggregate as extensively as the BSA–FITC powder. The confocal images suggest that PUR/PLGA-S scaffolds presented two barriers to diffusion, the

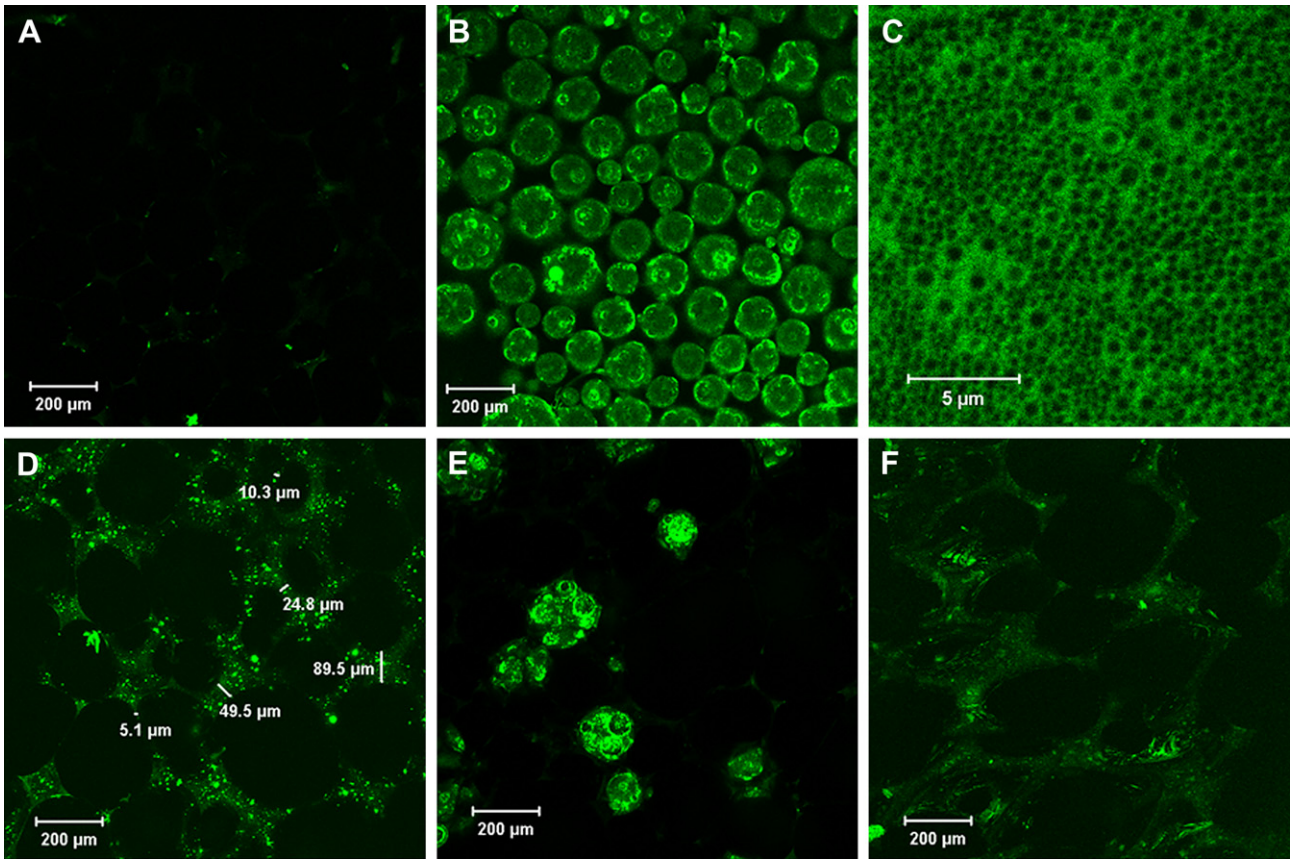

Fig. 4. Confocal microscopy images of PLGA microspheres and PUR scaffolds. (A) Blank PUR, (B) PLGA-L-BSA-FITC, (C) PLGA-S-BSA-FITC, (D) PUR/BSA-FITC, (E) PUR/PLGA-L-BSA-FITC, and (F) PUR/PLGA-S-BSA-FITC.

PLGA microspheres and the PUR pore wall, which was anticipated to substantially reduce the burst release [32].

3.4. In vitro release profile of rhBMP-2 from polyurethane scaffolds

Release profiles for rhBMP-2 encapsulated in PUR scaffolds and PLGA microspheres are presented in Fig. 5A. When rhBMP-2 was added to the scaffolds as a lyophilized powder, a burst release of 36% was observed on day 1, followed by a period of sustained release until day 21. As anticipated, microencapsulation of rhBMP-2 in PLGA-L and PLGA-S microspheres substantially decreased the burst release to <15%. However, the burst release surprisingly increased from 8% for PLGA-L-rhBMP-2 microspheres to 25% for the PUR/PLGA-L-rhBMP-2 scaffold. We have observed similar effects for BSA–FITC and tobramycin (unpublished results). As discussed previously, it is conjectured that the reaction exotherm promotes interfacial mixing of PUR and PLGA chains and subsequent diffusion of rhBMP-2 into the PUR phase during cure. These effects may be exacerbated by the observation that the distribution of the hydrophilic drug is weighted toward the surface [33]. In contrast to the PLGA-L-rhBMP-2 microspheres, encapsulation of PLGA-S-rhBMP-2 microspheres in PUR scaffolds was observed to reduce the burst release from 13% to 3%, which supports the hypothesis that embedding of PLGA-S microspheres in the pore walls of the scaffold increases the resistance to mass transfer.

The daily release profiles were calculated by fitting the cumulative release profile to a logarithm function as shown in Fig. 5B, where the differences in the amount of rhBMP-2 released in the first 12 days between the three delivery systems are clearly evident. The presence of 50% PEG in the polyester triol before reacting with isocyanate resulted in a higher burst and cumulative release (Fig. 5C), which is conjectured to result from enhanced diffusivity and/or solubility of the protein within the scaffold due to the hydrophilic PEG component [41].

Cumulative release curves measured for non-PEG containing foams (Fig. 5A) were fit to a power law model [34,35]:

$$M_t/M_0 = A \cdot t^n \tag{2}$$

Fitting parameters are listed in Table 4. In this model, M_t is the cumulative amount of rhBMP-2 released at time t, M_0 is the total amount of rhBMP-2 released (assumed to be the dose of rhBMP-2 added to the material), A is a constant, and n is the reaction order associated with the release. Values of n lower than 0.5 have been reported for porous materials [34], and a n value near 0.5 indicates a Fickian diffusion mechanism [34,35]. For the data shown in Fig. 5, the values of n were determined to be 0.21, 0.72, 0.30, 0.33, and 0.55 for PUR/BMP-2, PLGA-L-BMP2, PUR/PLGA-L-BMP-2, PLGA-S-BMP-2 and PUR/PLGA-S-BMP-2 materials, respectively. Encapsulation of PLGA-L-BMP-2 microspheres in the PUR scaffolds decreased the value of n. However, encapsulation of PLGA-S microspheres in PUR scaffolds increased the value of n from 0.33 to approximately 0.5, suggesting a diffusion-controlled release mechanism. When $n = 0.5$, Eq. (1) reduces to the Higuchi equation [42], where A is defined as follows:

$$A = [C_{sat} D(2C_{load} - C_{sat})]^{1/2} \tag{3}$$

In Eq. (3), C_{sat} = saturation concentration of the drug, C_{load} = loading concentration of the drug (e.g., the dose of rhBMP-2 added to

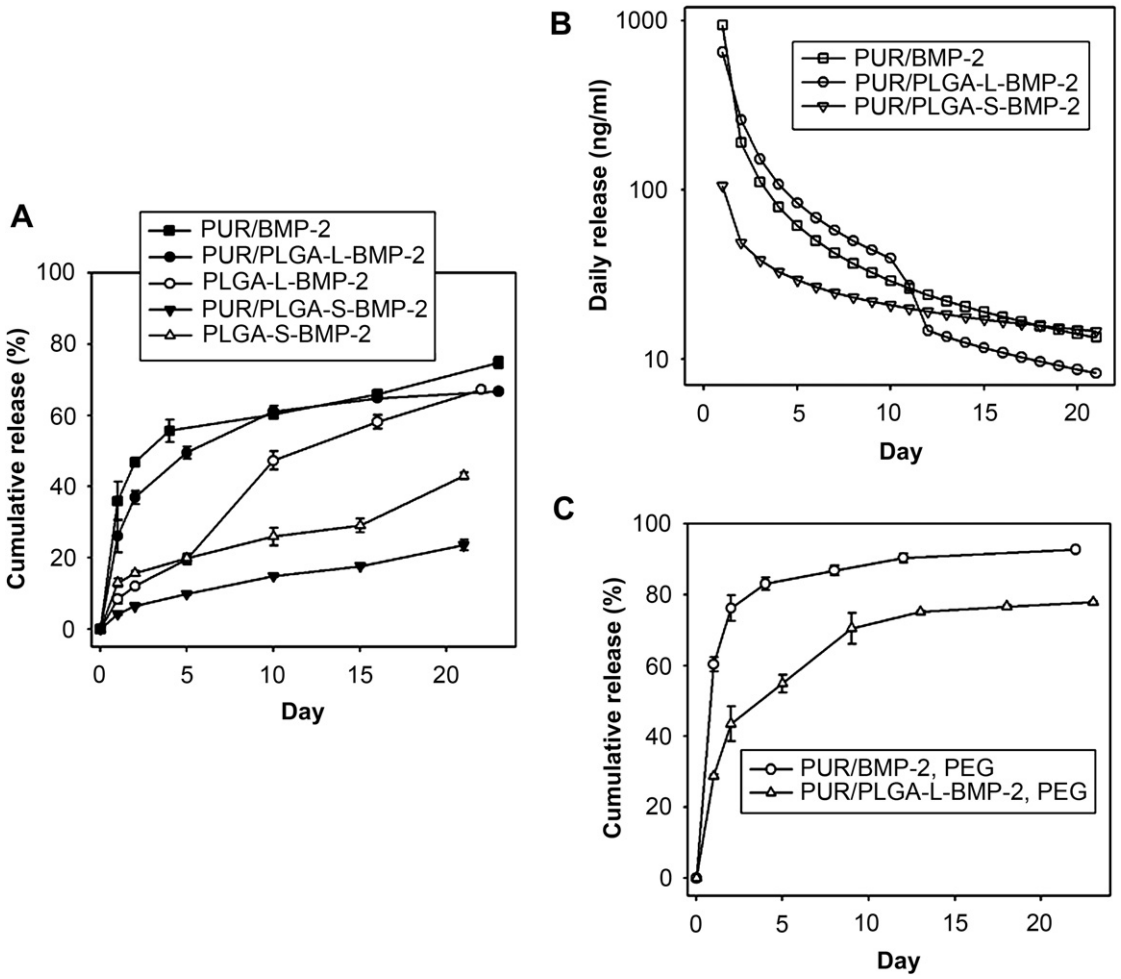

Fig. 5. In vitro release of rhBMP-2. (A) Cumulative release from PUR scaffolds and PLGA microspheres, (B) daily release from PUR scaffolds, and (C) cumulative release from scaffolds incorporating 50% PEG. Release kinetics were measured by ELISA.

the material), and D = the diffusivity of the drug in the polymer. When the PLGA-S-rhBMP-2 microspheres were embedded in the PUR scaffold, the value of A decreased from 12.2 to 4.2, which is consistent with the notion that the diffusivity of rhBMP-2 is lowest in these materials due to the two polymeric barriers (e.g., PLGA and PUR) to mass transfer.

3.5. In vitro bioactivity of released rhBMP-2

To verify the bioactivity of released rhBMP-2 from PUR scaffolds, the releasates were tested for ALP activity using MC3T3 cells. Both rhBMP-2 releasates from PUR/rhBMP-2 and PUR/PLGA-L-rhBMP-2 scaffolds significantly enhanced ALP activity at day 3 and day 7, when compared to the negative control (Fig. 6). There is no significant difference between the releasates and the fresh rhBMP-2 in terms of ALP activity. These results suggest that the osteoinductive potential of the rhBMP-2 was preserved during the chemical reaction associated with the foaming process.

Table 4
Parameters obtained by fitting rhBMP-2 release data to the power law model. M_t/M_0, t, A, and R^2 represent cumulative percentage released (%), time (day), constant, and the coefficient of determination, respectively.

$M_t/M_0 = D \cdot t^n$	n Value	A	R^2
PUR/rhBMP-2	0.21	38.60	0.952
PUR/PLGA-L-rhBMP-2	0.30	28.57	0.959
PLGA-L-rhBMP-2	0.72	7.65	0.977
PUR/PLGA-S-rhBMP-2	0.55	4.24	0.997
PLGA-S-rhBMP-2	0.33	12.17	0.942

3.6. In vivo study of rhBMP-2 scaffolds in rat femoral plug defects

To evaluate the *in vivo* osteoinductivity of PUR scaffolds incorporating rhBMP-2, cylindrical PUR scaffolds were implanted into rat femoral plug defects (Fig. 7A). At week 2, μCT analysis showed that both PUR/rhBMP-2 and PUR/PLGA-L-rhBMP-2 materials enhanced bone ingrowth near the bottom surface of the implant compared to the control with no rhBMP-2 (Fig. 7B). Conversely, there was no significant increase in new bone formation in PUR/PLGA-S-rhBMP-2 implants, presumably due to the relatively low cumulative amount of rhBMP-2 released at 2 weeks. At week 4, substantial new bone formation was visible throughout the entire volume of the implants in all treatment groups (Fig. 7C). The most extensive bone ingrowth was observed in PUR/rhBMP-2 samples, which exhibited formation of new cortex. Although the amount of bone ingrowth in PUR/PLGA-S-rhBMP-2 scaffolds at week 2 was relatively small, there was significantly more new bone formation in these scaffolds relative to the control at week 4, which is conjectured to result from sustained release of rhBMP-2. In the quantitative μCT analysis at week 4 (Fig. 8), the volume of new bone

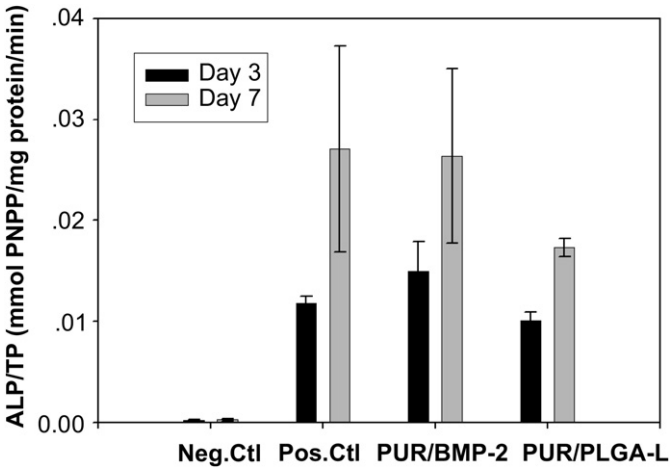

Fig. 6. In vitro alkaline phosphatase activity assay of rhBMP-2 releasates from PUR scaffolds. MC3T3 cells were treated with or without 100 ng/ml rhBMP-2 released from PUR scaffolds and ALP activity was measured at days 3 and 7. Fresh rhBMP-2 solution (100 ng/ml) was used as a positive control, and serum media containing no rhBMP-2 was used as the negative control.

formation per total scaffold volume (BV/TV, %) was significantly higher for all the rhBMP-2 treatment groups than the control ($p < 0.05$). Furthermore, new bone formation in the PUR/rhBMP-2 materials was significantly higher than that observed for the PUR/PLGA-rhBMP-2 treatment groups.

3.7. Histological analysis of PUR implants

Since μCT images only reveal the presence of mineralized bone [43], histological analysis was performed to give a more detailed analysis on the new bone tissue formation promoted by rhBMP-2 at early stage when the bone cells are not yet mineralized. In the histological analysis at week 2, bone ingrowth (the red areas within implants, highlighted in the high magnitude image with yellow arrows) from the surrounding tissue was enhanced in the rhBMP-2 treatment groups compared to the control (Fig. 9). At week 4, a substantial amount of mature bone formation was observed throughout the entire area of the rhBMP-2 implants, whereas new bone formation was observed only at the peripheral area in the control group (Fig. 9). New bone formation in the scaffold was most extensive in the PUR/rhBMP-2 materials, which is consistent with the μCT analysis. Histomorphometry data show that the rhBMP-2 treatment groups promoted new bone tissue formation significantly both at week 2 and week 4 (Fig. 10, $p < 0.05$). PUR/rhBMP-2

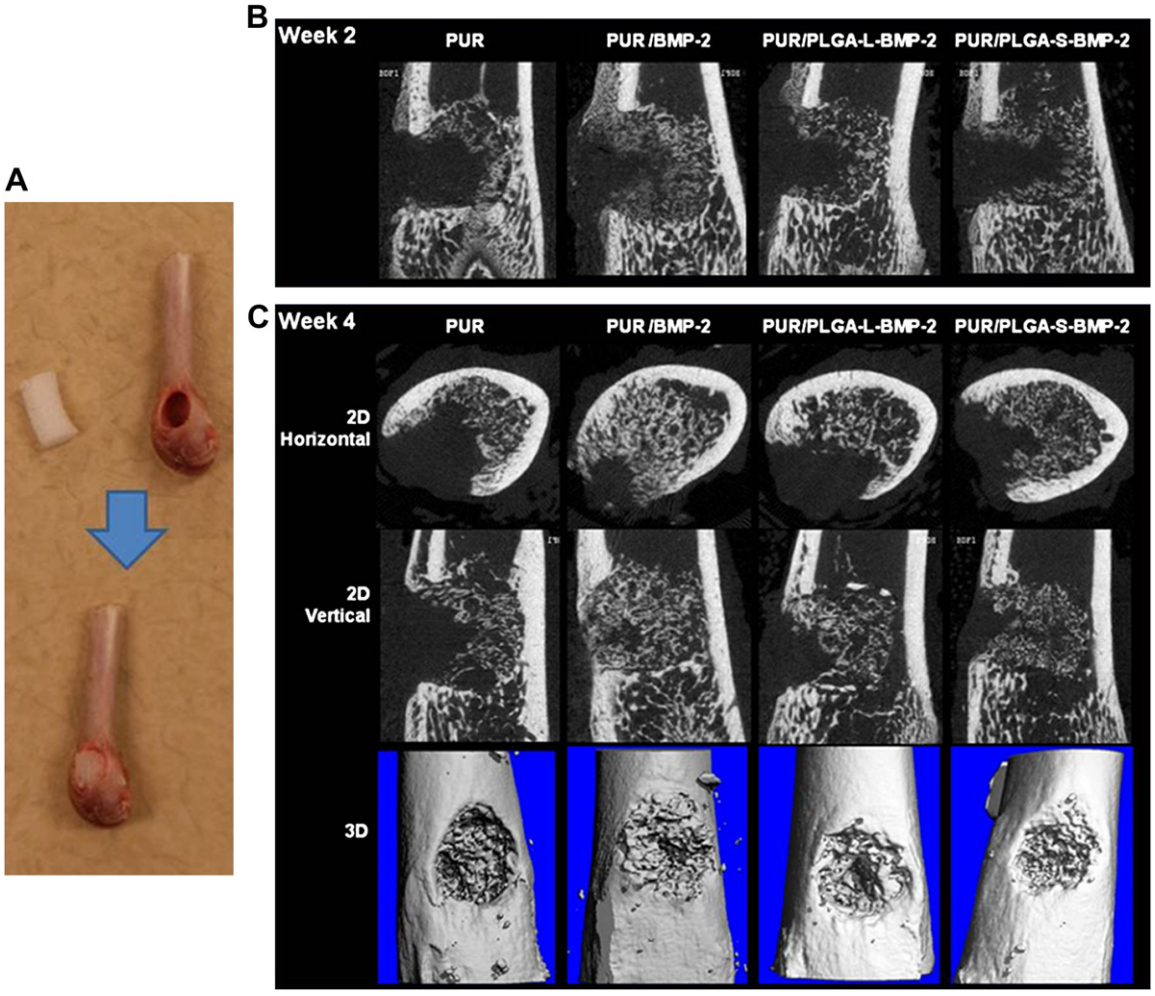

Fig. 7. In vivo evaluation of the effects of PUR/rhBMP-2 scaffolds on new bone formation in a rat femoral plug model. Treatment groups included: PUR control (no rhBMP-2), PUR/rhBMP-2, PUR/PLGA-L-rhBMP-2, and PUR/PLGA-S-rhBMP-2. The PUR cylinders (5 mm × 3 mm) were implanted into rat femoral plug defects (A), and harvested for μCT imaging at weeks 2 (B) and 4 (C) respectively.

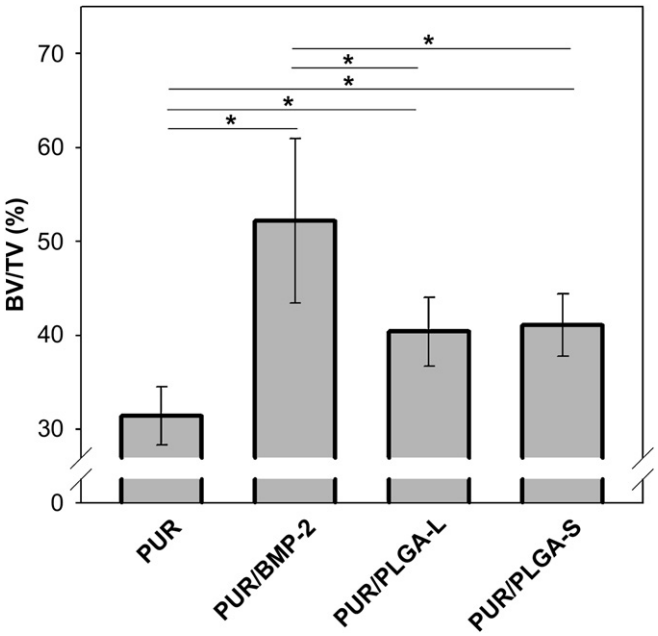

Fig. 8. Quantitative analysis of mineralized new bone formation from μCT images promoted by PUR/rhBMP-2, PUR/PLGA-L-rhBMP-2, and PUR/PLGA-S-rhBMP-2 scaffolds. The percentage of bone volume (BV) relative to total volume (TV) of each implant was assessed from μCT imaging. Stars and lines indicate significance differences between groups ($p < 0.05$).

seems to perform slightly better than the other two treatment groups although no statistically significant differences were observed.

4. Discussion

Biodegradable polyurethanes have been investigated extensively in tissue engineering as supportive scaffolds for cell attachment, growth, and differentiation. In recent studies, scaffolds fabricated from segmented PUR elastomers comprising hexamethylene diisocyanate (HDI) have been reported to support bone healing in iliac crest defects in sheep at six months [8,24]. In another study, two-component lysine-diisocyanate (LDI)-based biomaterials incorporating 10 wt% β-TCP (5 μm) were implanted and injected into femoral cortical defects in sheep [9]. Direct apposition of the biomaterial and bone was observed, as well as ingrowth of new bone into adjacent pores. Similarly, the materials investigated in the present study supported ingrowth of new bone into the plug as early as 2 weeks, with increased new bone formation at 4 weeks, as shown in Figs. 7–10. These results suggest that the two-component PUR scaffolds support bone ingrowth, which is in agreement with previous studies.

Considering the moderate osteoconductivity of PUR scaffolds, as well as their demonstrated ability to deliver biologically active molecules, we reasoned that release of rhBMP-2 would increase new bone formation and accelerate healing *in vivo*. In the present study, we report that the release of rhBMP-2 from PUR scaffolds is

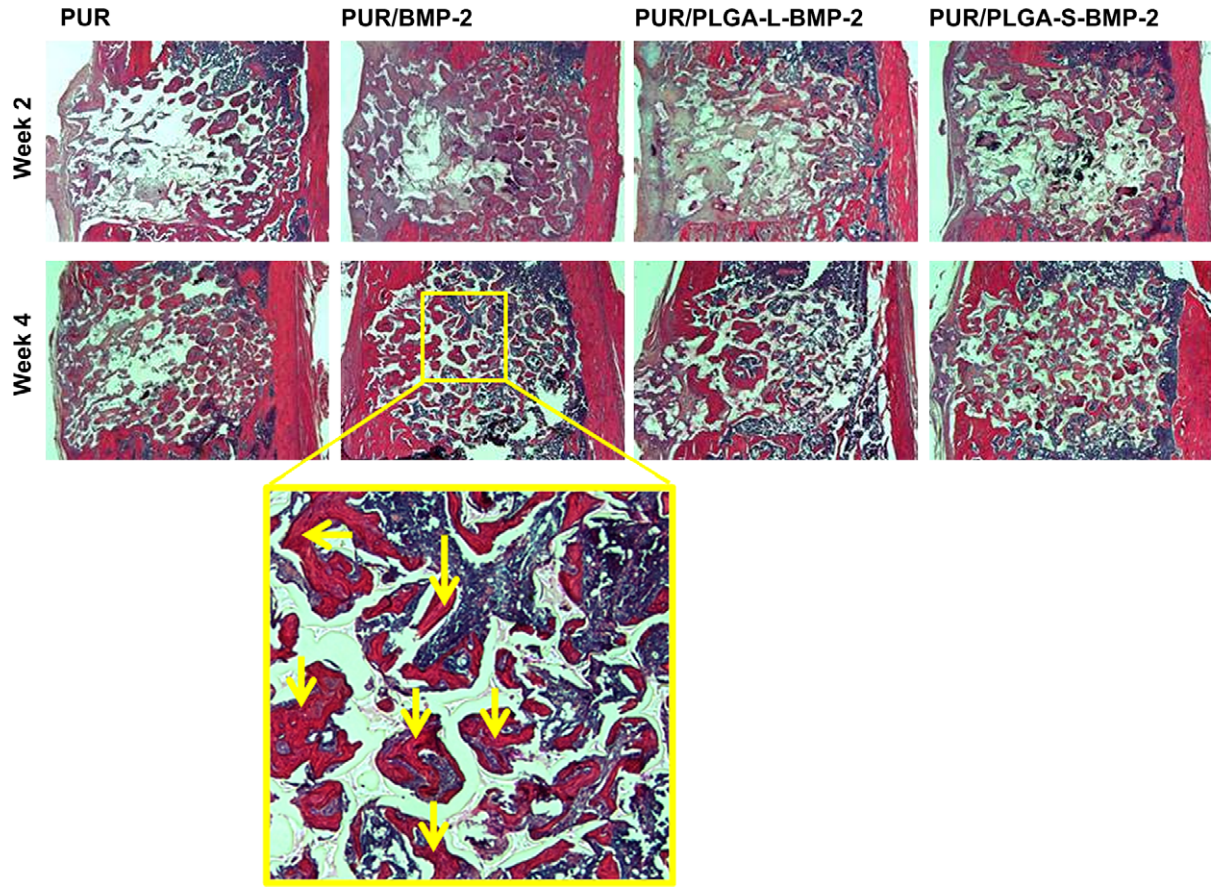

Fig. 9. Histological evaluation of new bone formation promoted by PUR/rhBMP-2, PUR/PLGA-L-rhBMP-2, and PUR/PLGA-S-rhBMP-2 scaffolds. Explanted bones were fixed in formalin, decalcified in EDTA, embedded in paraffin, and processed for H&E staining. The yellow arrows point to areas in the high magnitude images representing new bone formation.

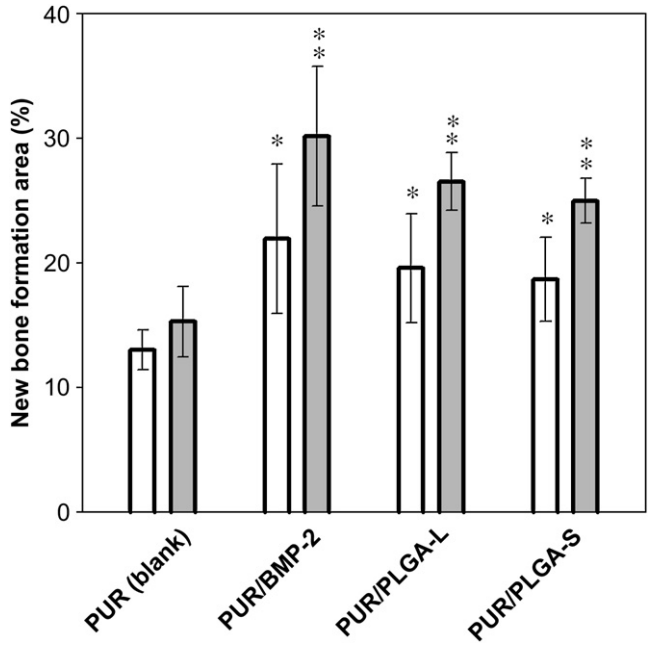

Fig. 10. Histomorphometric analysis of new bone formation promoted by PUR/rhBMP-2, PUR/PLGA-L-rhBMP-2, and PUR/PLGA-S-rhBMP-2 scaffolds at weeks 2 (hollow bars) and 4 (filled bars). Areas of new bone formation were highlighted using Photoshop elements 7.0 and then measured using Scion imaging software. Single stars indicate significance differences between treatment groups and the negative control (no rhBMP-2) at week 2, and double stars indicate significance differences between treatment groups and the negative control at week 4 ($p < 0.05$).

tunable by adopting different delivery strategies, and that the release profile affects the extent of cellular infiltration and new bone formation in a rat femoral plug model. In the simplest approach, rhBMP-2 powder was encapsulated in a two-component reactive PUR scaffold to investigate the effects of the chemical reaction on the bioactivity of rhBMP-2. PUR/rhBMP-2 scaffolds exhibited a burst release for the first few days followed by sustained release for approximately 15 days. Addition of PEG600 diol to the polyol component had a significant effect on the burst release. In the absence of PEG, the burst release for rhBMP-2 was only 36% compared to 60% for scaffolds incorporating 50 wt% PEG in the polyol component. Covalently bound PEG in the polymer network renders it more hydrophilic, which increases the swelling of the polymer and thus accelerates the release rate [41]. Furthermore, the cumulative release of rhBMP-2 from the 50% PEG scaffolds increased from 75% (no PEG) to 95%. In contrast, although the burst release of rhPDGF from PUR scaffolds incorporating PEG was also 60%, the cumulative release at day 21 was only 70% [2]. It has been suggested that the unfavorable conditions of the polymerization reaction may adversely affect the bioactivity of unprotected growth factors (e.g., by microencapsulation) [32]. However, the bioactivity of the rhBMP-2 powder was preserved, as evidenced by the *in vitro* data (Fig. 6) and the observation that PUR/rhBMP-2 scaffolds promoted a large amount of new bone formation relative to the negative control as early as 2 weeks.

A number of recent studies have shown that sustained release of rhBMP-2 enhances healing relative to a bolus release. Therefore, we sought to reduce the burst release observed for PUR/rhBMP-2 scaffolds by investigating the effects of PLGA microsphere size on rhBMP-2 release kinetics and new bone formation in the rat femoral plug model. We reasoned that encapsulation of rhBMP-2 in microspheres would reduce the burst release due to the increased resistance to mass transfer [32], but anticipated that this effect would diminish with increasing size. Our results show that microsphere size significantly affected the *in vitro* release kinetics. The PLGA-S microspheres were completely embedded in the scaffold, and the release of rhBMP-2 was observed to follow diffusion-controlled Fickian mass-transfer kinetics with essentially no burst [34,35]. Furthermore, embedding the PLGA-S microspheres in the PUR scaffolds decreased the release kinetics compared to that from the microspheres alone. These observations are in agreement with previous studies reporting that rhBMP-2 loaded PLGA/Hap particles [19] and PLGA nanospheres embedded in fibrin gels exhibited slower release compared to directly embedding the protein in the fibrin gel [44]. In other studies, incorporation of rhBMP-2-loaded PLGA and poly(propylene fumarate) (PPF) microspheres in reactive PPF scaffolds resulted in a more sustained release with a lower burst phase compared to rhBMP-2 impregnated scaffolds [18,45]. Additionally, Texas red dextran (TRD) encapsulated in PLGA (33 μm) and PPF (43 μm) microspheres that were subsequently encapsulated in PPF scaffolds exhibited a lower burst release relative to that from the microspheres themselves [32].

In contrast, the PLGA-L microspheres were only partially embedded in the scaffolds due to the fact that their size was comparable to the thickness of the pore walls. Furthermore, the T_g data suggest that the reaction exotherm promoted interfacial mixing, so that the burst release of protein actually increased when the PLGA-L microspheres were embedded in the scaffolds. A previous study has shown that the release of TRD from PPF microspheres embedded in PPF scaffolds was significantly slower that that from embedded PLGA microspheres due to crosslinking at the PPF microsphere/PPF scaffold interface [32]. These studies suggest that the composition of the interface affects the release kinetics – while interfacial crosslinking presents an additional barrier to mass transfer, interfacial mixing reduces the resistance to mass transfer. Taken together, these observations suggest that the release of rhBMP-2 from microsphere composite scaffolds depends on both the size of the microspheres as well as the compositions of the microspheres and scaffold.

The *in vitro* drug release profile has also been shown to relate to new bone formation *in vivo* [19,44]. In the present study, the release of rhBMP-2 was measured *in vitro* using a perfect sink model (e.g., all the release medium was removed daily) [46] due to the concern that released rhBMP-2 could degrade over time. It has been shown that although the release of rhBMP-2 was accelerated *in vivo* relative to *in vitro* conditions, the differences between treatment groups were similar [18,45]. In the rat femoral plug defect model with the selected dosage of 2.5 μg rhBMP-2 per implant, the burst release from PUR/rhBMP-2 promoted new mineralized bone formation as early as week 2 (Fig. 7B). The PUR/PLGA-L-rhBMP-2 scaffolds, which exhibited a burst release of 25% (compared to 35% for the PUR/rhBMP-2 formulation), also promoted more new bone formation relative to the control, but the amount of new bone was less than the PUR/rhBMP-2 formulation. The cumulative release from the PUR/rhBMP-2 scaffolds exceeded that from the PUR/PLGA-L-rhBMP-2 scaffolds until day 10, and at day 21 the cumulative release was comparable. This suggests that early release of rhBMP-2 is important for promoting new bone formation, which is in agreement with previous studies. BMP-2 has been reported to recruit human mesenchymal progenitor cells (MPCs) that are essential for bone development, remodeling, and repair [22]. In a recent study, rhBMP-2 delivered from Matrigel plugs has been reported to promote angiogenesis in severe combined immunodeficient (SCID) mice via both canonical and noncanonical Wnt pathways [21]. The role of BMP-2 in fracture healing has also been investigated. Over a 28-day period of fracture healing in mouse tibias, mRNA expression of BMP-2 was highest on day 1 post-fracture, which suggests that BMP-2 may function as the trigger in

the fracture healing cascade that regulates the expression of other BMPs [23].

The PUR/PLGA-S-rhBMP-2 treatment group, which yielded no burst release, promoted the least amount of new bone formation compared to the other two rhBMP-2 treatment groups. However, a significant amount of new bone formation in PUR/PLGA-S-rhBMP-2 scaffolds between weeks 2 and 4 suggests that sustained release is also important to promote new bone formation. This observation is in agreement with a fracture healing study reporting that injection of rhBMP-2 in a calcium phosphate carrier at one week after surgery enhanced healing in a primate osteotomy model relative to percutaneous injection within one day [20]. The improvement in healing observed for the delayed injection treatment group has been attributed to an increased number of cells that respond to the released rhBMP-2. The importance of a sustained release of rhBMP-2 is also underscored by previous studies showing that sustained release of rhBMP-2 protein from polymer scaffolds promoted more bone formation in both orthotopic [19] and ectopic [18,44] models relative to a bolus release.

The bolus release of rhBMP-2 in the first several hours [16] may contribute to the requirement of high rhBMP-2 dosage in clinical studies when delivered by a collagen sponge (INFUSE® Bone Graft) [47,48]. Due to the fact that BMP-2 is a potent morphogen, there are safety issues associated with administering high levels of the drug [49,50]. Therefore, to mitigate the risk associated with high dosages and reduce the amount of the expensive growth factor that must be delivered to achieve a therapeutic effect, it is desirable to control the release of rhBMP-2 in order to optimize new bone formation. Our findings suggest that both early and sustained release of rhBMP-2 are critical in order to promote optimal bone wound healing, which is consistent with the multiple roles of this growth factor in bone formation. In an alternative approach, dual delivery of rhVEGF and rhBMP-2 synergistically enhanced bone regeneration relative to either factor alone [51,52], presumably due to enhanced angiogenesis and recruitment of cells to the wound site. It is interesting to note that there was a significant burst release of rhVEGF and minimal burst release of rhBMP-2 in at least one of these studies [51]; thus it is likely that the effects of rhBMP-2 on cell recruitment and angiogenesis at the early time points were minimal compared to rhVEGF. Considering the multiple roles of rhBMP-2 in bone healing at both early and late time points, optimizing its release may present compelling opportunities to maximize bone formation with just one growth factor, which is simpler from a regulatory perspective than the dual growth factor approach. Since the femoral plug defect heals spontaneously within 8 weeks [53], the optimal rhBMP-2 release strategy for healing more challenging defects cannot be identified from the present study. In ongoing studies, we are investigating the effects of the rhBMP-2 delivery strategy on bone healing in critical-size femoral segmental defects in rats, which may require a greater fraction of the growth factor to be delivered over longer time scales. Although the relative proportions of rhBMP-2 released at early and later time points have not been optimized for healing defects more challenging than the femoral plug, the data suggest that both a burst followed by sustained release of rhBMP-2 are important for promoting new bone formation.

5. Conclusion

Biodegradable PUR scaffolds incorporating rhBMP-2 prepared by reactive liquid molding promoted new bone formation in a rat femoral plug model. The burst release of rhBMP-2 was reduced by encapsulating the rhBMP-2 in PLGA microspheres prior to the foaming reaction, and both microsphere size and composition were observed to affect rhBMP-2 burst release and new bone formation. Our observations suggest that both a burst release within the first several days as well as sustained release for up to 3 weeks is important to enhance formation of new bone tissue.

Acknowledgement

This work was funded by the Orthopaedic Trauma Research Program (DOD-W81XWH-07-1-0211), the Armed Forces Institute of Regenerative Medicine (sub-contract from the Rutgers-Cleveland Clinic Consortium Award DOD-W81XWH-08-2-0034), Vanderbilt University School of Engineering, and the Vanderbilt Center for Bone Biology. The authors also thank Professor Jeffrey Hollinger at Carnegie Mellon University for the gift of rhBMP-2.

Appendix

Figures with essential colour discrimination. Certain figures in this article, in particular Figs. 4, 7 and 9, have parts that are difficult to interpret in black and white. The full colour images can be found in the on-line version, at doi:10.1016/j.biomaterials.2009.08.038.

References

[1] Bennett S, Connolly K, Lee DR, Jiang Y, Buck D, Hollinger JO, et al. Initial biocompatibility studies of a novel degradable polymeric bone substitute that hardens in situ. Bone 1996;19(1):S101–7.
[2] Li B, Davidson JM, Guelcher SA. The effect of the local delivery of platelet-derived growth factor from reactive two-component polyurethane scaffolds on the healing in rat skin excisional wounds. Biomaterials 2009;30(20):3486–94.
[3] Zhang JY, Beckman EJ, Hu J, Yang GG, Agarwal S, Hollinger JO. Synthesis, biodegradability, and biocompatibility of lysine diisocyanate-glucose polymers. Tissue Eng 2002;8(5):771–85.
[4] Guan JJ, Sacks MS, Beckman EJ, Wagner WR. Synthesis, characterization, and cytocompatibility of elastomeric, biodegradable poly(ester-urethane)ureas based on poly(caprolactone) and putrescine. J Biomed Mater Res 2002;61(3):493–503.
[5] Santerre JP, Woodhouse K, Laroche G, Labow RS. Understanding the biodegradation of polyurethanes: from classical implants to tissue engineering materials. Biomaterials 2005;26(35):7457–70.
[6] Fujimoto KL, Guan J, Oshima H, Sakai T, Wagner WR. In vivo evaluation of a porous, elastic, biodegradable patch for reconstructive cardiac procedures. Ann Thorac Surg 2007;83(2):648–54.
[7] Fujimoto KL, Tobita K, Merryman WD, Guan J, Momoi N, Stolz DB, et al. An elastic, biodegradable cardiac patch induces contractile smooth muscle and improves cardiac remodeling and function in subacute myocardial infarction. J Am Coll Cardiol 2007;49(23):2292–300.
[8] Gorna K, Gogolewski S. Preparation, degradation, and calcification of biodegradable polyurethane foams for bone graft substitutes. J Biomed Mater Res Part A 2003;67A(3):813–27.
[9] Adhikari R, Gunatillake PA, Griffiths I, Tatai L, Wickramaratna M, Houshyar S, et al. Biodegradable injectable polyurethanes: synthesis and evaluation for orthopaedic applications. Biomaterials 2008;29(28):3762–70.
[10] Guelcher S, Srinivasan A, Hafeman A, Gallagher K, Doctor J, Khetan S, et al. Synthesis, In vitro degradation, and mechanical properties of two-component poly(ester urethane)urea scaffolds: effects of water and polyol composition. Tissue Eng 2007;13(9):2321–33.
[11] Guelcher SA. Biodegradable polyurethanes: synthesis and applications in regenerative medicine. Tissue Eng Part B Rev 2008;14(1):3–17.
[12] Guelcher SA, Patel V, Gallagher KM, Connolly S, Didier JE, Doctor JS, et al. Synthesis and in vitro biocompatibility of injectable polyurethane foam scaffolds. Tissue Eng 2006;12(5):1247–59.
[13] Hafeman AE, Li B, Yoshii T, Zienkiewicz K, Davidson JM, Guelcher SA. Injectable biodegradable polyurethane scaffolds with release of platelet-derived growth factor for tissue repair and regeneration. Pharm Res 2008;25(10):2387–99.
[14] Hafeman AE, Zienkiewicz KJ, Davidson JM, Guelcher SA. Injectability of biodegradable, porous polyurethane scaffolds for tissue regeneration. TERMIS-NA 2008 annual conference; Abstract 2008.
[15] Guan J, Stankus JJ, Wagner WR. Biodegradable elastomeric scaffolds with basic fibroblast growth factor release. J Control Release 2007;120(1–2):70–8.
[16] Jeon O, Song SJ, Kang SW, Putnam AJ, Kim BS. Enhancement of ectopic bone formation by bone morphogenetic protein-2 released from a heparin–conjugated poly(L-lactic-co-glycolic acid) scaffold. Biomaterials 2007;28(17):2763–71.

[17] Jeon O, Kang SW, Lim HW, Chung JH, Kim BS. Long-term and zero-order release of basic fibroblast growth factor from heparin-conjugated poly (L-lactide-co-glycolide) nanospheres and fibrin gel. Biomaterials 2006;27(8): 1598–607.
[18] Kempen DH, Kruyt MC, Lu L, Wilson CE, Florschutz AV, Creemers LB, et al. Effect of Autologous BMSCs Seeding and BMP-2 Delivery on ectopic bone formation in a microsphere/poly(propylene fumarate) composite. Tissue Eng Part A 2008;15(3):587–94.
[19] Kim SS, Gwak SJ, Kim BS. Orthotopic bone formation by implantation of apatite-coated poly(lactide-co-glycolide)/hydroxyapatite composite particulates and bone morphogenetic protein-2. J Biomed Mater Res A 2008;87(1): 245–53.
[20] Seeherman H, Li R, Bouxsein M, Kim H, Li XJ, Smith-Adaline EA, et al. rhBMP-2/calcium phosphate matrix accelerates osteotomy-site healing in a nonhuman primate model at multiple treatment times and concentrations. J Bone Joint Surg Am 2006;88(1):144–60.
[21] de Jesus Perez VA, Alastalo TP, Wu JC, Axelrod JD, Cooke JP, Amieva M, et al. Bone morphogenetic protein 2 induces pulmonary angiogenesis via Wnt-beta-catenin and Wnt-RhoA-Rac1 pathways. J Cell Biol 2009;184(1): 83–99.
[22] Fiedler J, Roderer G, Gunther KP, Brenner RE. BMP-2, BMP-4, and PDGF-bb stimulate chemotactic migration of primary human mesenchymal progenitor cells. J Cell Biochem 2002;87(3):305–12.
[23] Cho TJ, Gerstenfeld LC, Einhorn TA. Differential temporal expression of members of the transforming growth factor beta superfamily during murine fracture healing. J Bone Miner Res 2002;17(3):513–20.
[24] Gorna K, Gogolewski S. Biodegradable polyurethanes for implants. II. In vitro degradation and calcification of materials from poly(epsilon-caprolactone)-poly(ethylene oxide) diols and various chain extenders. J Biomed Mater Res 2002;60(4):592–606.
[25] Betz MW, Caccamese JF, Coletti DP, Sauk JJ, Fisher JP. Tissue response and orbital floor regeneration using cyclic acetal hydrogels. J Biomed Mater Res A 2008;99A(3):819–29.
[26] Hoshino M, Egi T, Terai H, Namikawa T, Kato M, Hashimoto Y, et al. Repair of long intercalated rib defects in dogs using recombinant human bone morphogenetic protein-2 delivered by a synthetic polymer and beta-tricalcium phosphate. J Biomed Mater Res A 2008;99A(2):514–21.
[27] Kempen DH, Yaszemski MJ, Heijink A, Hefferan TE, Creemers LB, Britson J, et al. Non-invasive monitoring of BMP-2 retention and bone formation in composites for bone tissue engineering using SPECT/CT and scintillation probes. J Control Release 2008;134(3):169–76.
[28] Kim S, Kim SS, Lee SH, Eun Ahn S, Gwak SJ, Song JH, et al. In vivo bone formation from human embryonic stem cell-derived osteogenic cells in poly (D, L-lactic-co-glycolic acid)/hydroxyapatite composite scaffolds. Biomaterials 2008;29(8):1043–53.
[29] Kim SE, Jeon O, Lee JB, Bae MS, Chun HJ, Moon SH, et al. Enhancement of ectopic bone formation by bone morphogenetic protein-2 delivery using heparin-conjugated PLGA nanoparticles with transplantation of bone marrow-derived mesenchymal stem cells. J Biomed Sci 2008;15(6):771–7.
[30] Kirker-Head C, Karageorgiou V, Hofmann S, Fajardo R, Betz O, Merkle HP, et al. BMP-silk composite matrices heal critically sized femoral defects. Bone 2007;41(2):247–55.
[31] Takahashi Y, Yamamoto M, Tabata Y. Enhanced osteoinduction by controlled release of bone morphogenetic protein-2 from biodegradable sponge composed of gelatin and beta-tricalcium phosphate. Biomaterials 2005; 26(23):4856–65.
[32] Kempen DH, Lu L, Kim C, Zhu X, Dhert WJ, Currier BL, et al. Controlled drug release from a novel injectable biodegradable microsphere/scaffold composite based on poly(propylene fumarate). J Biomed Mater Res A 2006;77(1):103–11.
[33] Berkland C, Kipper MJ, Narasimhan B, Kim KK, Pack DW. Microsphere size, precipitation kinetics and drug distribution control drug release from biodegradable polyanhydride microspheres. J Control Release 2004;94(1):129–41.
[34] Benita S. Microencapsulation: methods and industrial applications. 2nd ed. CRC Press; 2006.
[35] Siepmann J, Peppas NA. Modeling of drug release from delivery systems based on hydroxypropyl methylcellulose (HPMC). Adv Drug Deliv Rev 2001;48(2–3):139–57.
[36] Karp JM, Rzeszutek K, Shoichet MS, Davies JE. Fabrication of precise cylindrical three-dimensional tissue engineering scaffolds for in vitro and in vivo bone engineering applications. J Craniofac Surg 2003;14(3):317–23.
[37] Torigoe I, Sotome S, Tsuchiya A, Yoshii T, Maehara H, Sugata Y, et al. Bone regeneration with autologous plasma, bone marrow stromal cells, and porous beta-tricalcium phosphate in nonhuman primates. Tissue Eng Part A 2009; 15(7):1489–99.
[38] Oldham JB, Lu L, Zhu X, Porter BD, Hefferan TE, Larson DR, et al. Biological activity of rhBMP-2 released from PLGA microspheres. J Biomech Eng 2000; 122(3):289–92.
[39] Forcino RG, Jonnalagadda S. The effect of fabrication methods on the mechanical and thermal properties of poly(lactide-co-glycolide) scaffolds. J Appl Polym Sci 2007;104(2):944–9.
[40] www.triton-technology.co.uk/pdf/TTAN_016.pdf.
[41] Hafeman AE, Zienkiewicz KJ, Carney E, Litzner B, Stratton C, Wenke JC, et al. Local delivery of tobramycin from injectable biodegradable polyurethane scaffolds. J Biomater Sci 2009, doi:10.1163/156856209X410256.
[42] Higuchi T. Rate of release of medicaments from ointment bases containing drugs in suspension. J Pharm Sci 1961;50:874–5.
[43] Sawyer AA, Song SJ, Susanto E, Chuan P, Lam CX, Woodruff MA, et al. The stimulation of healing within a rat calvarial defect by mPCL-TCP/collagen scaffolds loaded with rhBMP-2. Biomaterials 2009;30(13):2479–88.
[44] Jeon O, Song SJ, Yang HS, Bhang SH, Kang SW, Sung MA, et al. Long-term delivery enhances in vivo osteogenic efficacy of bone morphogenetic protein-2 compared to short-term delivery. Biochem Biophys Res Commun 2008;369(2):774–80.
[45] Kempen DH, Lu L, Hefferan TE, Creemers LB, Maran A, Classic KL, et al. Retention of in vitro and in vivo BMP-2 bioactivities in sustained delivery vehicles for bone tissue engineering. Biomaterials 2008;29(22):3245–52.
[46] Saarinen-Savolainen P, Jarvinen T, Taipale H, Urtti A. Method for evaluating drug release from liposomes in sink conditions. Int J Pharm 1997;159(1):27–33.
[47] Boyne PJ, Marx RE, Nevins M, Triplett G, Lazaro E, Lilly LC, et al. A feasibility study evaluating rhBMP-2/absorbable collagen sponge for maxillary sinus floor augmentation. Int J Periodontics Restorative Dent 1997;17(1):11–25.
[48] Howell TH, Fiorellini J, Jones A, Alder M, Nummikoski P, Lazaro M, et al. A feasibility study evaluating rhBMP-2/absorbable collagen sponge device for local alveolar ridge preservation or augmentation. Int J Periodontics Restorative Dent 1997;17(2):124–39.
[49] Hoffmann A, Weich HA, Gross G, Hillmann G. Perspectives in the biological function, the technical and therapeutic application of bone morphogenetic proteins. Appl Microbiol Biotechnol 2001;57(3):294–308.
[50] Hogan BL. Bone morphogenetic proteins: multifunctional regulators of vertebrate development. Genes Dev 1996;10(13):1580–94.
[51] Kempen DH, Lu L, Heijink A, Hefferan TE, Creemers LB, Maran A, et al. Effect of local sequential VEGF and BMP-2 delivery on ectopic and orthotopic bone regeneration. Biomaterials 2009;30(14):2816–25.
[52] Patel ZS, Young S, Tabata Y, Jansen JA, Wong ME, Mikos AG. Dual delivery of an angiogenic and an osteogenic growth factor for bone regeneration in a critical size defect model. Bone 2008;43(5):931–40.
[53] Nie H, Ho ML, Wang CK, Wang CH, Fu YC. BMP-2 plasmid loaded PLGA/HAp composite scaffolds for treatment of bone defects in nude mice. Biomaterials 2009;30(5):892–901.